THE ASTROPHYSICAL JOURNAL, 547:574–589, 2001 February 1

HALO PROPERTIES IN COSMOLOGICAL SIMULATIONS OF SELF-INTERACTING COLD DARK MATTER

ROMEEL DAVÉ[1,2] AND DAVID N. SPERGEL[3]
Princeton University Observatory, Princeton, NJ 08544
AND
PAUL J. STEINHARDT[4] AND BENJAMIN D. WANDELT[5]
Department of Physics, Princeton University, Princeton, NJ 08544
Received 2000 June 15; accepted 2000 September 28

ABSTRACT

We present a comparison of halo properties in cosmological simulations of collisionless cold dark matter (CDM) and self-interacting dark matter (SIDM) for a range of dark matter cross sections. We find, in agreement with various authors, that CDM yields cuspy halos that are too centrally concentrated as compared to observations. Conversely, SIDM simulations using a Monte Carlo N-body technique produce halos with significantly reduced central densities and flatter cores. We introduce a concentration parameter based on enclosed mass that we expect will be straightforward to determine observationally and present predictions for SIDM and CDM. SIDM also produces more spherical halos than CDM, providing possibly the strongest observational constraint on SIDM. In our simulations with SIDM cross sections $\sigma_{\rm DM} \approx 10^{-23}$ to 10^{-25} cm^2 GeV^{-1}, collisions reduce the central density in galaxy halos, with larger cross sections producing lower densities. Simulations in the upper end of this range best match current observations of galaxy properties but are disfavored by cluster simulations of Yoshida and colleagues. This problem would be alleviated in models in which the cross section is velocity dependent.

Subject headings: cosmology: theory — dark matter — galaxies: formation — galaxies: halos — methods: n-body simulations

1. INTRODUCTION

The cold dark matter (CDM) family of cosmological models provides an excellent description of a wide variety of observational results, from the earlier observable epochs detected via microwave background fluctuations to present-day observations of galaxies and large-scale structure. A "concordance model" with roughly one-third matter and two-thirds vacuum energy, either a cosmological constant or quintessence (Caldwell, Dave, & Steinhardt 1998), is consistent with almost all current observations on scales $\gtrsim 1$ Mpc (Bahcall et al. 1999).

Recently, improving observations and numerical techniques has enabled a comparison of CDM scenarios to observations on galactic scales of approximately a few kiloparsecs. The results have not been encouraging. There are a number of distinct observations that may be in conflict with predictions of CDM:

1. The density profile of galaxies in the inner few kiloparsecs appears to be much shallower than predicted by numerical simulations (Navarro, Frenk, & White 1997, hereafter NFW97). For density profiles characterized by $\rho(r) \propto r^{\alpha}$ as $r \to 0$, CDM predicts $\alpha \approx -1.5$ with little scatter (Moore et al. 1999b), while current Hα observations suggest $\alpha \approx -0.5$ with significant scatter (Swaters, Madore, & Trewhella 2000; Dalcanton & Bernstein 2000; although see van den Bosch & Swaters 2000).
2. The central density of dark matter halos is observed to be $\rho_c \sim 0.02\ M_{\odot}\ {\rm pc}^{-3}$ roughly independent of halo mass (Firmani et al. 2000b), while CDM predicts halos with $\rho_c \gtrsim 1\ M_{\odot}\ {\rm pc}^{-3}$ at dwarf galaxy masses, increasing to larger masses (Moore et al. 1999b).
3. The number of dwarf galaxies in the Local Group is significantly fewer than predicted by CDM simulations, with the discrepancy growing toward smaller masses (Moore et al. 1999a; Klypin et al. 1999).
4. Hydrodynamic simulations produce galaxy disks that are too small and have too little angular momentum (Navarro & Steinmetz 2000).
5. The robustness of rapidly rotating bars in high surface brightness spiral galaxies implies lower density cores than predicted by CDM (Debattista & Sellwood 1998).
6. Cluster CL 0024+1654 is nearly spherical with a large, soft core, while CDM typically predicts triaxial clusters with cuspy cores (Tyson, Kochanski, & Dell'antonio 1998; although see Miralda-Escudé 2000 for a counter example).

Each piece of evidence taken individually is perhaps not convincing enough to claim that CDM has failed on galactic scales. For instance, until recently there was controversy among simulators regarding inner profiles (Kravtsov et al. 1998), but more careful simulations have converged on a consistent prediction (Klypin 2000). Observationally, inner galactic profiles are uncertain as a result of beam smearing effects in H I observations (Swaters et al. 2000; van den Bosch et al. 2000), though samples of high-resolution Hα observations continue to show shallower profiles than predicted by CDM (Dalcanton & Bernstein 2000). The number of observed Local Group dwarf galaxies may be reconciled with CDM via plausible scenarios for suppressed galaxy formation (e.g., Bullock, Kravtsov, & Weinberg 2000), compact high-velocity clouds could represent the "missing

[1] rad@astro.princeton.edu.
[2] Spitzer Fellow.
[3] dns@astro.princeton.edu.
[4] steinh@princeton.edu.
[5] bwandelt@princeton.edu.

satellites" that are seen in N-body simulations (Blitz et al. 1999), or else the dark halo masses of Local Group dwarfs may be systematically underestimated. Hydrodynamic simulations of disk galaxy formation are fraught with the usual concerns about the effects of feedback, artificial viscosity, and resolution, though it appears that the discrepancies above are due to the underlying dark matter distribution (Navarro & Steinmetz 2000).

It becomes more interesting to consider alternatives to conventional CDM when one recognizes that all of these discrepancies may be symptomatic of a single cause: *dark matter halos in CDM simulations appear to be more centrally concentrated than observed.* Recognizing this, various authors have recently forwarded a plethora of alternative dark matter theories that suppress the central concentration of dark matter in galaxy halos. Some such theories are that the dark matter is warm (Sommer-Larsen & Dolgov 2000; Colín, Avila-Reese, & Valenzuela 2000; Hannestad & Scherrer 2000), repulsive (Goodman 2000), fluid (Peebles 2000), fuzzy (Hu, Barkana, & Gruzinov 2000), decaying (Cen 2000), annihilating (Riotto & Tkachev 2000; Kaplinghat, Knox, & Turner 2000), and the alternative we investigate here, self-interacting (SIDM; Spergel & Steinhardt 2000). Interestingly, all theories may be tuned to solve the problems mentioned above (at least in analytic approximations), all theories may be motivated from particle physics considerations, and all theories retain the desirable properties of CDM on extragalactic scales (though warm dark matter is nontrivially constrained by this requirement; see Narayanan et al. 2000).

SIDM is governed by a single free parameter, the cross section per unit mass $\sigma_{\rm DM}$ of the interacting dark matter particle. Spergel & Steinhardt (2000) suggested $\sigma_{\rm DM} \sim 10^{-22}$ to 10^{-25} cm^2 GeV^{-1} in order to reduce the central concentration of galaxy halos by a sufficient amount to alleviate the above problems. Intriguingly, this value is close to the cross section of ordinary hadrons, motivating some particular particle physics candidates for SIDM (Bento et al. 2000; P. J. Steinhardt et al. 2000, in preparation). If $\sigma_{\rm DM}$ is significantly smaller than this range, then the optical depth at galactic densities is much less than unity, implying that SIDM would have a negligible effect on the dark matter distribution in halos.

A qualitative picture of the evolution of an SIDM halo is as follows: At early times there is no difference between SIDM and CDM since the densities and peculiar velocities are sufficiently low that collisions are rare; hence, SIDM makes identical predictions to CDM regarding cosmic microwave background fluctuations and the Lyα forest. As the halo forms and grows via gravitational instability, the central density increases. Eventually, collisions are so frequent that dark matter particles scatter out of the center as fast as they are accreted, and the density growth is halted, forming a core. Such a limit is not present in the CDM model, where the central density grows unchecked. The SIDM core then begins to extend while retaining constant central density. Heat transfer from the outer parts of the halo raises the temperature in the halo core. If the halo is truly isolated, then eventually the core thermalizes with the exterior resulting in an isothermal halo with a steep density profile. This initiates gravothermal collapse, where the direction of heat transfer is reversed and the exterior begins to cool the halo center. However, in a realistic cosmological setting, galaxies constantly accrete material, keeping the outer halo hot and heat flowing inward, thus delaying core collapse. The interplay between collisional heat transfer and accretion determines whether a halo will undergo core collapse in a Hubble time.

It is important to appreciate that the transport behavior does not change monotonically with $\sigma_{\rm DM}$. For small cross sections, heat transfer increases with $\sigma_{\rm DM}$ since the frequency of collisions increases; however, for large cross sections, the conductivity $\kappa \propto \sigma_{\rm DM}^{-1} \rightarrow 0$ and no heat transfer occurs. Thus, as we discuss in § 6, the fluid approximation is a poor description of SIDM in the moderate cross section regime proposed by Spergel & Steinhardt (2000). Furthermore, the behavior in the moderate cross section regime cannot be surmised by interpolating between the fluid and the noninteracting CDM regimes. A proper treatment of the SIDM proposal, which includes the interplay of accretion and heat transfer, its nonmonotonic dependence $\sigma_{\rm DM}$, and the effects of merging, demands numerical simulations designed to explore the moderate cross section regime.

In this paper we investigate the statistical properties of halos in SIDM and CDM in cosmological N-body simulations. Our spatial and mass resolutions are sufficient to probe the inner regions ($\sim 1\ h^{-1}$ kpc) of small halos ($\gtrsim$ a few times $10^9\ M_\odot$), while maintaining sufficient volume so as to have a significant sample of such halos. We use a Monte Carlo technique similar to Kochanek & White (2000) to model collisions. The primary difference between our simulations and prior investigations (discussed in more detail in § 6) is that we model a cosmologically significant random volume of the universe with self-interaction cross sections in the range favored by Spergel & Steinhardt (2000), enabling us to characterize the statistical properties of halos as we vary $\sigma_{\rm DM}$.

Section 2 describes our initial conditions and simulation techniques using a Monte Carlo N-body approach. In § 3 we compare the structural properties of halos in CDM versus SIDM models with several cross sections. In particular, we examine their central densities, inner profile slopes α, the mass dependence of α, concentrations, phase space densities, and ellipticities, and where possible we compare to observations. In § 4 we use lower resolution simulations to test the effects of finite particle numbers in our Monte Carlo method. In § 5 we examine the subhalo population around the largest halo in our simulations. In § 6 we compare our findings to the simulations of other groups who have conducted numerical studies of self-interacting dark matter and examine results from a wider range of $\sigma_{\rm DM}$. We summarize our results and discuss observational constraints in § 7. We find that SIDM with $\sigma_{\rm DM} \approx 10^{-23}$ to 10^{-24} cm^2 GeV^{-1} produces galaxy halos that are in better agreement than collisionless CDM for a wide variety of observations.

2. SIMULATING SIDM

2.1. *Code and Cosmology*

We use a modified version of GADGET (Springel, Yoshida, & White 2000), a publicly available tree code with smoothed particle hydrodynamics (SPH) for distributed-memory parallel machines. Here we only employ the gravitational N-body portion. We evolve a $4\ h^{-1}$ Mpc randomly chosen volume of a ΛCDM universe with $\Omega = 0.3$, $\Omega_\Lambda = 0.7$, $H_0 = 70$ km s^{-1} Mpc^{-1}, and $\sigma_8 = 0.8$, similar to the "concordance model" in agreement with a wide variety of observations (Bahcall et al. 1999). We generate initial condi-

TABLE 1

SIMULATION RESULTS

MODEL	σ_{DM} (cm^2 GeV^{-1})	128^3*				64^3†			
		N_{halo}	α_{med}	$\rho_{c,med}$[a]	$c_{M,med}$	N_{halo}	α_{med}	$\rho_{c,med}$[a]	$c_{M,med}$
CDM	0	670	−1.49	1.95	8.0	111	−1.58	1.91	6.7
SIDM	10^{-24}	647	−0.93	0.22	5.6	106	−1.44	0.36	4.8
SIDM	10^{-23}	566	−0.37	0.030	2.6	89	−0.53	0.027	1.8
Observed.....	...	...	≈ -0.5	≈ 0.02	...	...	≈ -0.5	≈ 0.02	...

NOTE.—Asterisk denotes 128^3 median values computed for all halos with greater than 1000 particles (~ 30 per run). Dagger denotes 64^3 median values computed for all halos with greater than 500 particles (~ 10 per run).

[a] Central dark matter density in $M_\odot$ pc^{-3}; values shown are extrapolated from 1 to 0.5 h^{-1} kpc using α_{median}.

tions using COSMICS (Ma & Bertschinger 1995) at $z = 49.7$, while our particle distribution is still in the linear regime, and evolve to $z = 0$. We employ 128^3 dark matter particles in each run, resulting in a dark matter particle mass of $m_p = 3.6 \times 10^6\ M_\odot$ and a spline kernel softening of $\epsilon = 1\ h^{-1}$ kpc (i.e., force is Newtonian at 2ϵ). To test resolution effects, we also run a suite of simulations with 64^3 particles and $\epsilon = 2\ h^{-1}$ kpc. Their initial conditions have an initial density field identical to the 128^3 runs, constructed by sampling at alternate grid points.

While our $4\ h^{-1}$ Mpc box is small, well below the nonlinear scale at $z = 0$ (it goes nonlinear around $z \sim 3$), we are interested here in the behavior on scales of a few kiloparsecs, and it is unlikely that the missing large-scale power would have a significant effect on the inner portions of halos. It does imply, however, that galaxy clustering will not be accurately modeled in this volume, which may have some impact on halo shapes, as we will discuss in § 3.7. The merger history of halos, especially the largest ones in our volume, is significantly altered by the lack of large-scale power, and this could in principle have some effect on halo profiles. We further caution that the profile statistics presented here may have large cosmic variance, so our comparisons to observations should be regarded as preliminary. Nevertheless, our primary conclusions are based on a comparative study between collisionless and collisional dark matter for individual halos, so we expect these results to be robust to volume effects.

2.2. *Modeling Self-Interactions*

We have modified GADGET to include self-interactions using a Monte Carlo N-body technique to probabilistically incorporate collisions, along the same lines as Burkert (2000) and Kochanek & White (2000), closer to the latter as we use $\Delta \boldsymbol{v}$ from individual particles colliding rather than setting $\Delta \boldsymbol{v}$ to be the particle's velocity (see the discussion in Kochanek & White 2000). Each pair of particles with positions and velocities $(\boldsymbol{r}_1, \boldsymbol{v}_1)$ and $(\boldsymbol{r}_2, \boldsymbol{v}_2)$, separated by $\delta x \equiv |\boldsymbol{r}_1 - \boldsymbol{r}_2|/(2\epsilon)$ and $\delta v \equiv |\boldsymbol{v}_1 - \boldsymbol{v}_2|$, interacts with a probability given by

$$P = f_{\rm geom}(\delta x)\,\frac{\delta v\,\Delta t}{\lambda}\,, \tag{1}$$

where Δt is the time step,

$$\lambda = \frac{4\pi(2\epsilon)^3}{3m_p}\,\frac{1}{\sigma_{\rm DM}}\,, \tag{2}$$

and

$$f_{\rm geom}(\delta x) = N\,\frac{\int_0^1 W(\delta x)W(\delta x + \delta x')d(\delta x')}{\int_0^1 W^2(\delta x')d(\delta x')}\,, \tag{3}$$

where W is the cubic spline kernel used in GADGET. This geometrical factor weights the probability of interaction by the product of spline kernel–weighted density distributions of the two particles at their given separation. The normalization N is set by requiring that

$$\int_0^1 f_{\rm geom}(\delta x) 4\pi\,\delta x^2\,d(\delta x) = 1\,, \tag{4}$$

which ensures that when a particle has interacted with all its neighbors within 2ϵ, the resulting probability is equivalent to

$$P = \sigma_{\rm DM}\,\rho\,\delta v\,\Delta t\,, \tag{5}$$

where ρ is the local dark matter density.

In our code, the scatterings are performed between individual particles at the time that the acceleration between those particles is being computed (i.e., during the "treewalk"). In order to ensure that all possible scatterings are considered, a tree cell is opened whenever it is within 2ϵ of a particle, regardless of the opening criterion.

If two particles scatter, their velocities are randomly reoriented, keeping the magnitudes of their velocities fixed. In practice, a running sum is kept of the change in velocity due to the interactions that a given particle undergoes on every processor, and at the end of the step the velocity change for each particle is summed over all processors and added to that particle's velocity. In this way, energy and momentum are explicitly conserved, even if the scattered particles are on different processors or a particle undergoes more than one scatter in a single time step (which is very rare for the cross sections considered here).

We consider $\sigma_{\rm DM} = 0$ (collisionless), 10^{-24}, and 10^{-23} cm^2 GeV^{-1}. We also examined $\sigma_{\rm DM} = 10^{-25}$ cm^2 GeV^{-1} and $\sigma_{\rm DM} = 10^{-22}$ cm^2 GeV^{-1} in a 64^3 simulation, which we will examine in § 6. The total number of collisions per particle in our simulations is 1.01 for $\sigma_{\rm DM} = 10^{-24}$ cm^2 GeV^{-1} and 6.05 for $\sigma_{\rm DM} = 10^{-23}$ cm^2 GeV^{-1}, with slightly lower numbers (0.9 and 5.3) for the 64^3 runs. Note that a factor of 10 increase in $\sigma_{\rm DM}$ translates only to a factor of 6 increase in the number of collisions, since the lowered central densities (§ 3.2) partially compensate for the increase in $\sigma_{\rm DM}$. All runs were performed on Fluffy, a 32 processor Beowulf-class machine at Princeton, with each 128^3 run taking approximately 1 week.

2.3. *The Simulated Halo Sample*

We identify dark matter halos using SKID[6] (Spline Kernel Interpolative DENMAX; see Katz, Weinberg, & Hernquist 1996), with a linking length of 2ϵ. We only consider halos containing 64 or more particles, to ensure a roughly complete sample of such halos in our simulations (Weinberg et al. 1999). Table 1 lists the number of halos identified in these simulations.

A specific resolution issue arises from the finite number of particles used to model collisions in the SIDM simulations probabilistically: the number of particles in a given halo must be high enough to Monte Carlo–sample the distribution properly. As we will show in § 4, halos with $\gtrsim 1000$ particles at $z = 0$ seem to be accurately represented with this technique for the simulations considered here. This is quite restrictive but still permits a significant sample of halos (roughly 30 in each 128^3 run) with which to compute statistics. We also use the full sample of halos to examine certain aspects, but we will be cautious about interpretations made from halos below this "Monte Carlo resolution limit."

[6] http://www-hpcc.astro.washington.edu/tools/SKID.

3. HALO STRUCTURE

3.1. *Halo Profiles*

We determine halo profiles $\rho(r)$ by spherical averages over radii $r = \epsilon$–30ϵ, in 20 equal intervals of log r. A sample of 16 halo profiles from our 128^3 simulations is shown in Figure 1. Each panel shows a halo profile for $\sigma_{\rm DM} = 0$ (*solid lines*), 10^{-24} (*short-dashed lines*), and 10^{-23} cm^2 GeV^{-1} (*long-dashed lines*). Dotted line segments emanating from the innermost radius point of the $\sigma_{\rm DM} = 0$ curve indicate slopes $\alpha = -0.5$, -1, and -1.5 for comparison. The same corresponding halos are chosen from each simulation, allowing a case-by-case comparison of the effect of SIDM. The outer halo profiles ($r \gtrsim 10\,h^{-1}$ kpc) are virtually identical for each halo, showing that the effects of self-interactions are limited to the inner few kiloparsecs of halos and confirming that the same halos are being compared in the dif-

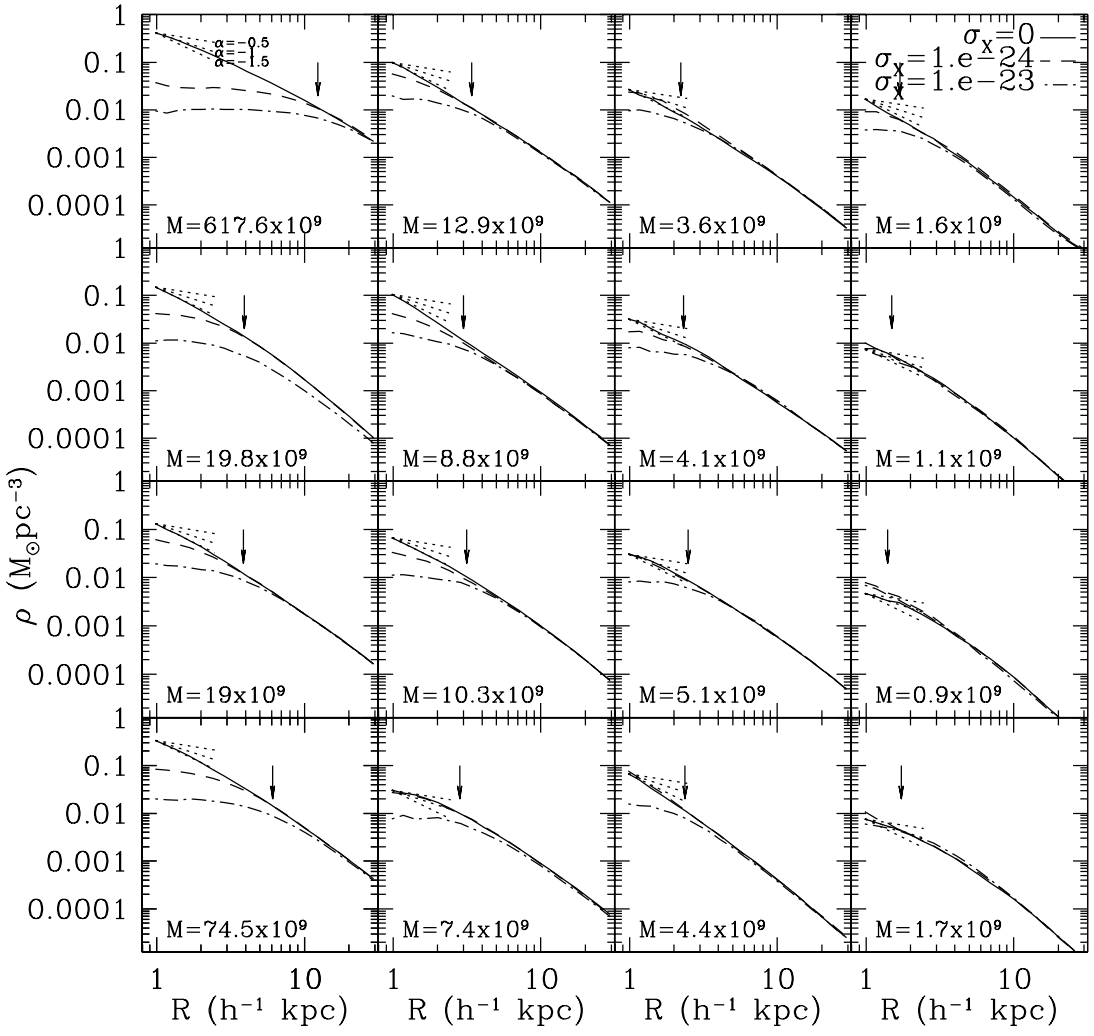

FIG. 1.—Sample of 16 selected halo profiles for collisionless (*solid lines*), 10^{-24} cm^2 GeV^{-1} (*dashed lines*), and 10^{-23} cm^2 GeV^{-1} (*dot-dashed lines*). Corresponding halos from each simulation are presented, allowing a direct comparison of the effect of SIDM on a halo-by-halo basis. The total halo mass in $M_\odot$ for the $\sigma_{\rm DM} = 0$ halo is shown in the lower right; the SIDM halo masses are typically within 20%. Arrow indicates $0.1r_{200}$ for CDM halos. The columns are ordered by mass, with the four highest mass halos shown in the leftmost column. Dotted lines from the innermost point show reference slopes of $\alpha = -0.5$, -1.0, and -1.5.

ferent simulations. The halos in the leftmost column are the four most massive ones in our simulations, while the halos in other columns are chosen randomly from a descending range of masses. The arrows indicate 10% of the virial radius r_{200} for each halo, where $r_{200} = 0.0145(M_{\rm halo}/M_\odot)^{1/3}$ h^{-1} kpc (NFW97); note that in the self-interacting case, the halo core size scales roughly with r_{200}. Note that the rightmost column shows halos with roughly 300 particles each, below our Monte Carlo resolution requirement of $\gtrsim$1000 particles (i.e., $\gtrsim 3.6 \times 10^9\ M_\odot$), thus the effects of self-interactions are not necessarily accurately represented in these cases.

From Figure 1 it is immediately evident that SIDM produces halos that have enlarged central cores and shallower inner profiles. CDM halos are almost all cuspy ($\alpha \lesssim -1$ typically), while most $\sigma_{\rm DM} = 10^{-23}$ cm^2 GeV^{-1} cores are close to flat. A value of $\sigma_{\rm DM} = 10^{-24}$ cm^2 GeV^{-1} leads to profiles that are intermediate between these two. In some cases, noncuspy CDM halos are seen, especially at lower masses. In these cases the halo may have undergone recent merging activity that temporarily lowers the central density, which is particularly effective in smaller mass halos. Additionally, recent mergers that have not relaxed make it difficult to identify unambiguously the halo center about which to compute profiles, typically making profiles appear shallower. We make no cut in regard to the merging history or "isolatedness" of halos, but we do note that the missing large-scale power in our simulations will tend to generate fewer mergers and make the largest objects in our simulations appear more isolated.

At high masses, the effect of SIDM is very prominent. The upper leftmost halo is Milky Way sized ($6 \times 10^{11}\ M_\odot$) and shows a large core of $\sim 15\ h^{-1}$ kpc for $\sigma_{\rm DM} = 10^{-23}$ cm^2 GeV^{-1} ($\sim 8\ h^{-1}$ kpc for $\sigma_{\rm DM} = 10^{-24}$ cm^2 GeV^{-1}). The core size and difference in inner slope become less prominent to lower masses, though this could be due to the increasing effects of unrelaxed halos, as well as the Monte Carlo resolution issues discussed earlier. We examine these issues quantitatively in § 3.4.

No evidence is seen for SIDM halo profiles that are isothermal, as would be expected if the cross section was so large that core collapse would occur on timescales significantly shorter than a Hubble time. This supports the analytic estimates of Spergel & Steinhardt (2000) that core collapse on a Hubble time would not occur until $\sigma_{\rm DM} \gtrsim 10^{-22}$ cm^2 GeV^{-1}.

Overall, there is a clear trend on a case-by-case basis that SIDM results in a reduced central density and shallower inner slope of the dark matter halo, with increasing $\sigma_{\rm DM}$ having a greater such effect.

3.2. *Central Densities*

Figure 2 shows the central density of dark matter halos ρ_c, taken to be the density at our innermost resolved radius ϵ, as a function of halo mass. Here we only consider halos with more than 1000 particles, where our Monte Carlo technique has sufficient numbers to represent the collisional behavior (as we will discuss in § 4). The central halo density of galaxies is observed to be $\sim 0.02\ M_\odot$ pc^{-3} (Firmani et al. 2000b) and is consistent with being independent of halo mass. The observed range of halo densities is shown as the hatched region, with a majority of their data falling toward the lower end of that region. The arrow in the upper left indicates the increase in ρ_c projecting the profile from 1 h^{-1} kpc into 500 pc, typical of observations of dwarf and low surface brightness galaxy central densities, using the slope shown.

SIDM $\sigma_{\rm DM} = 10^{-23}$ cm^2 GeV^{-1} halos are in good agreement with these observations, while $\sigma_{\rm DM} = 10^{-24}$ cm^2 GeV^{-1} produces inner densities that are a few times higher but still marginally consistent with observations. In addition, ρ_c in SIDM models shows little trend with halo mass, in agreement with observations, because the core density is set by collisional physics.

Conversely, the more massive halos in CDM have central densities that are too high by at least an order of magnitude already at 1 h^{-1} kpc, and because of their cuspy profile, the disagreement would be much worse at smaller radii, as indi-

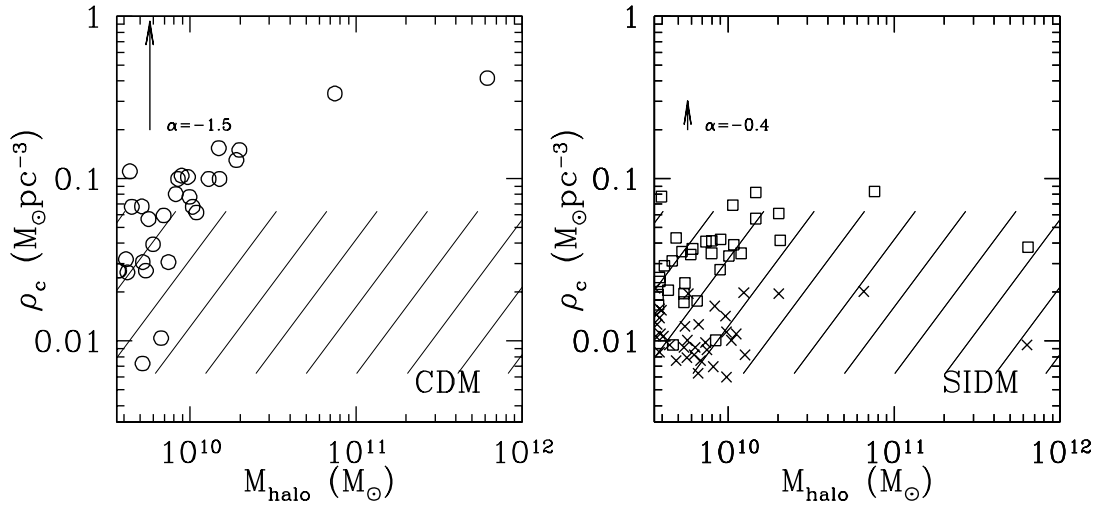

FIG. 2.—ρ_c vs. $M_{\rm halo}$ for CDM (*left panel*) and SIDM (*right panel*). For SIDM, crosses show $\sigma_{\rm DM} = 10^{-23}$ cm^2 GeV^{-1}, while open squares show $\sigma_{\rm DM} = 10^{-24}$ cm^2 GeV^{-1}. Only halos with 1000 or more particles are shown. The hatched region indicates the range of observed ρ_c compiled by Firmani et al. (2000a). Arrow in upper left indicates how much each value of ρ_c would increase if measured at 500 pc (instead of 1 h^{-1} kpc), typical of observations, assuming a profile with the slope shown.

cated by the arrow in the upper left. Moreover, CDM halos have central densities that increase with mass at a fixed radius, in conflict with observations. Note that this "trend" arises because we are considering the density at a fixed radius, as is more typically the case in observations. At a fixed fraction of the virial radius, the densities show no significant trend with mass; as seen in Figure 1, the densities at $0.1r_{200}$ are quite similar across all CDM halos.

SIDM halos appear to agree better with observations. Table 1 lists the median central density of halos with more than 1000 particles in our various models. This shows that our simulations reproduce the observed central halo densities for $\sigma_{\rm DM} \approx 10^{-23}$ cm^2 GeV^{-1}.

3.3. *Inner Profile Slopes*

We estimate the inner halo profile slope α as the slope between the innermost resolved radii, $r = 1$–$1.5\ h^{-1}$ kpc. In particular, this means we are not actually estimating the asymptotic inner slope of the density profile but rather the slope at a particular radius, $r \approx 1\ h^{-1}$ kpc. Figure 3 shows a histogram of this slope for the collisionless (*solid line*), 10^{-24} cm^2 GeV^{-1} (*dashed line*), and 10^{-23} cm^2 GeV^{-1} (*dot-dashed line*) cases, for all halos that have more than 1000 particles. The number of such halos in each simulation is indicated in the legend. The qualitative impression from Figure 1 that SIDM produces shallower inner profiles is quantified in Figure 3. The median values of α are indicated by the arrows from the upper x-axis and are listed in Table 1. CDM produces halos that have cuspy cores, with $\alpha_{\rm med} \approx -1.5$. A total of 25 out of the 28 CDM halos have $\alpha < -1$, indicating that cuspy cores are a common feature of CDM models. Conversely, the inner slopes in SIDM models are significantly shallower. For $\sigma_{\rm DM} = 10^{-24}$ cm^2 GeV^{-1}, $\alpha_{\rm med} \approx -0.9$, while for $\sigma_{\rm DM} = 10^{-23}$ cm^2 GeV^{-1}, $\alpha_{\rm med} \approx -0.4$, with no halos having $\alpha < -1$.

Our CDM profiles are, at face value, in better agreement with the analytic profile of Moore et al. (1999b), with an asymptotic slope of $\alpha = -1.5$, rather than an NFW97 profile having $\alpha(r \to 0) = -1$. However, profile fitting is a tricky business (as discussed in Klypin 2000). By reducing the scale radius in the NFW97 profile (i.e., increasing the concentration), one can push the transition to a slope of $\alpha = -1$ to a radius smaller than $1\ h^{-1}$ kpc where we cannot resolve the profiles (the "cusp-core degeneracy"; see van den Bosch & Swaters 2000). Thus, we suspect that our CDM profiles can also be adequately fitted by an NFW97 profile having a large concentration parameter. As such, we do not argue for or against either profile form. Our simulations can only predict the slope at $r \approx 1\ h^{-1}$ kpc, and that is what should be compared to observations. SIDM with $\sigma_{\rm DM} = 10^{-23}$ cm^2 GeV^{-1} has a median α close to the value preliminarily suggested by Hα observations of low surface brightness galaxies (Dalcanton & Bernstein 2000), though a definitive value awaits a more thorough analysis of observational biases. Note that these observations typically measure the slope at $\sim$500 kpc and thus may be more consistent with $\sigma_{\rm DM} = 10^{-24}$ cm^2 GeV^{-1} if the simulated profile continues to become shallower at $r < 1\ h^{-1}$ kpc.

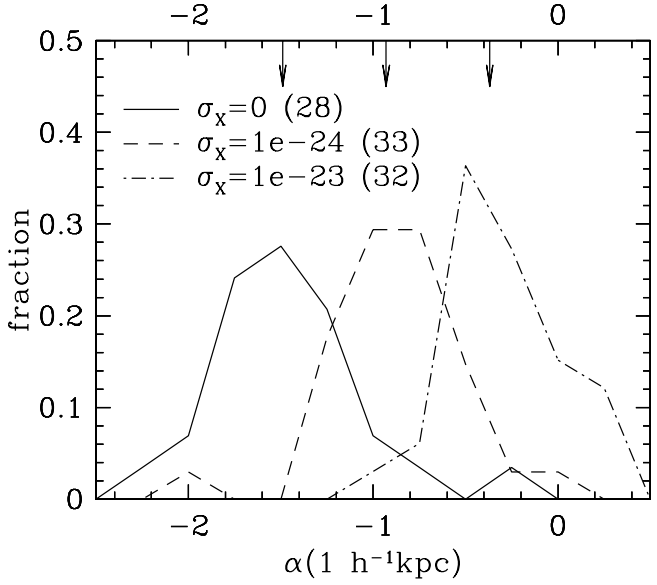

FIG. 3.—Histogram of inner slopes α for collisionless (*solid line*), 10^{-24} cm^2 GeV^{-1} (*dashed line*), and 10^{-23} cm^2 GeV^{-1} (*dot-dashed line*). Only halos with $M > 3.6 \times 10^9\ M_\odot$ (>1000 particles) are included; the number of such halos is indicated in parentheses in the figure. The median values of α are indicated by the arrows from the top edge of the plot and are listed in Table 1.

The scatter in α is mostly real. There is some scatter due to discreteness effects in measuring the inner slope as we do. While we could obtain an inner slope from fitting a general halo shape (Hernquist 1990; Klypin 2000), with five free parameters the inner slope would be poorly constrained by 20 correlated data points, thus we choose our simpler definition. Further scatter arises from recently merged halos that temporarily have shallower profiles until relaxed. However, neither of these effects is very significant for the high-mass halos plotted in Figure 3. Still, we choose to quote the median α rather than the mean, in order to quantify "typical" halos in these models and reduce sensitivity to outliers, although the mean is similar. We note that a significant scatter in inner slopes is also seen in the observations (e.g., de Blok, McGaugh, & van der Hulst 1996; Dalcanton & Bernstein 2000).

SIDM appears to be in better agreement with observations of the inner slopes of dark halo profiles than CDM. At face value, $\sigma_{\rm DM} = 10^{-23}$ cm^2 GeV^{-1} is preferred, but given uncertainties in observations and simulation techniques, $\sigma_{\rm DM} = 10^{-24}$ cm^2 GeV^{-1} is probably also consistent. A similar value of $\sigma_{\rm DM}$ also reproduces the observed central density of galaxies. Such a coincidence is not expected a priori and may represent a significant success of the SIDM scenario.

3.4. *Mass Dependence of Inner Slope*

Figure 4 shows a plot of inner halo slope α versus halo mass $M_{\rm halo}$ for all halos in our CDM (*left panel*) and SIDM (*right panel*; $\sigma_{\rm DM} = 10^{-23}$ cm^2 GeV^{-1}) simulations. The curve shows the running median value of α in bins of $\Delta(\log M) = 0.5$.

The CDM case shows almost no trend with mass, with the median slope always around -1.2 to -1.5. The largest halo does have a slightly shallower slope, consistent with the trend seen in very high resolution CDM simulations of individual halos (Jing & Suto 2000). The scatter increases to low mass as a result of discreteness and merging effects described in § 3.3.

The SIDM case shows dramatically different behavior, suggesting at face value that smaller halos have steeper inner profiles. However, caution must be used in interpreting this result. First, smaller halos have smaller cores,

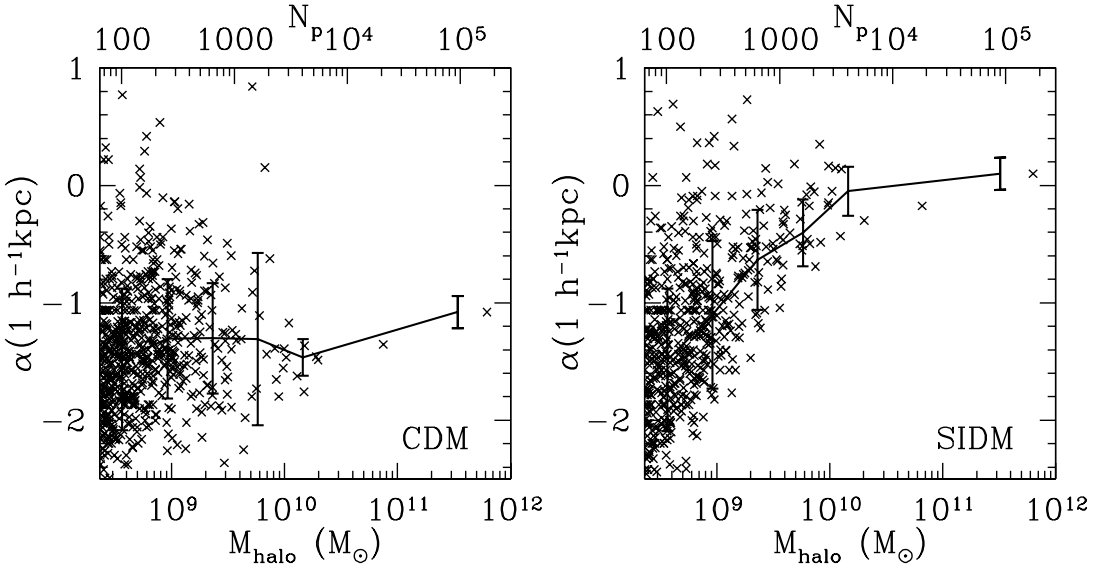

FIG. 4.—α vs. M_{halo} for CDM (*left panel*) and SIDM ($\sigma_{DM} = 10^{-23}$ cm^2 GeV^{-1}; *right panel*). All halos with 64 or more particles are shown. The line shows a running median of the α distribution, with a variance computed from all halos within each mass bin.

meaning that a slope measured at a fixed radius (not scaled to the halo core size) will result in a steeper slope. For CDM this effect is less significant, since the slope remains similar from the outer to the inner halo. Second, the small number of particles in the low-mass halos makes the Monte Carlo technique less effective in modeling collisions, thereby making SIDM appear more like CDM; we investigate this issue further in § 4. Thus, we make no claim regarding a trend of α with M_{halo}.

3.5. *Mass Concentration Parameter*

As seen in Figure 1, SIDM appears to have the desired effect of reducing the concentration of dark matter halos. In this section we quantify this effect using a concentration parameter, which we define differently than previous authors in order to facilitate a more direct comparison with observations.

The canonical definition of a concentration parameter is given by NFW97 as the ratio between the virial radius r_{200} (taken to be the radius at which the halo density is 200 times the cosmic mean) and the scale radius of the halo r_s in the NFW97 profile. This concentration parameter, however, is difficult to compute unambiguously in the case of non-isolated halos and difficult to compare directly to observations that seldom extend out to r_{200}. Furthermore, r_s is only defined within the context of the specific NFW97 model, and profile fits are typically degenerate between r_s and concentration (Klypin 2000). Colín et al. (2000) circumvent some of these issues by defining the concentration as the ratio of the minimum of r_{200} and the halo radius to the radius that encloses 20% of the halo mass. However, this inner radius is dependent on knowing the total halo mass, something that is difficult to determine observationally.

Instead, we choose to define a mass concentration parameter c_M, based on enclosed mass rather than radii, and restrict the scales in our definition to those where observations are available, typically $r \lesssim 20\ h^{-1}$ kpc. We define

$$c_M = 27\,\frac{M(<r_{in})}{M(<r_{out})}\,, \tag{6}$$

with

$$r_{in} = \frac{1}{3}\,r_{out} = 8.5\ \mathrm{kpc}\,\frac{v_{circ}}{220\ \mathrm{km\ s^{-1}}}\,, \tag{7}$$

where v_{circ} is the circular velocity of the halo. The choice of r_{in} is arbitrary; here we base it on the Milky Way, as it is convenient and results in observationally accessible scales. The scaling with v_{circ} is that expected for self-similar halos following the Tully-Fisher relation. The normalization factor of 27 results in a uniform density distribution having a mass concentration of unity. A flat rotation curve between r_{in} and r_{out} implies $M(r) \propto r$, resulting in $c_M = 9$. In our simulations, we take v_{circ} to be the maximum circular velocity of the halo as output by SKID.

Figure 5 shows a histogram of c_M for all halos with more than 1000 particles. As expected, there is a clear trend for CDM to have more concentrated halos than SIDM, with the amount of concentration decreasing with increasing σ_{DM}. Note that the difference between SIDM with 10^{-24} and 10^{-23} cm^2 GeV^{-1} is exaggerated relative to the difference between the inner slopes of those models (see Fig. 3). This is because the concentration is increased in 10^{-24} cm^2 GeV^{-1} relative to 10^{-23} cm^2 GeV^{-1}, both as a result of the increased inner slope as well as the reduced core radius. We also examined the mass dependence of c_M and found no obvious trend, but our range of masses is small.

For comparative purposes, our mass concentration parameter c_M may be analytically related to the NFW97 concentration parameter c_{NFW}. From NFW97,

$$\frac{v_c^2(x)}{v_{200}^2} = \frac{1}{x}\,\frac{\ln(1 + c_{NFW}\,x) - c_{NFW}\,x/(1 + c_{NFW}\,x)}{\ln(1 + c_{NFW}) - c_{NFW}/(1 + c_{NFW})}\,, \tag{8}$$

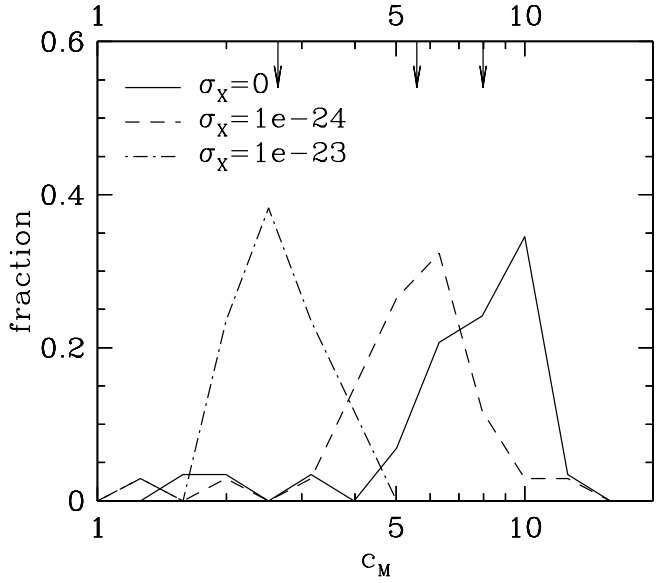

FIG. 5.—Histogram of mass concentrations c_M for collisionless (*solid line*), 10^{-24} cm^2 GeV^{-1} (*dashed line*), and 10^{-23} cm^2 GeV^{-1} (*dot-dashed line*). Only halos with $M > 3.6 \times 10^9\ M_\odot$ (>1000 particles) are included. The median values of c_M are indicated by the arrows from the top edge of the plot and are listed in Table 1.

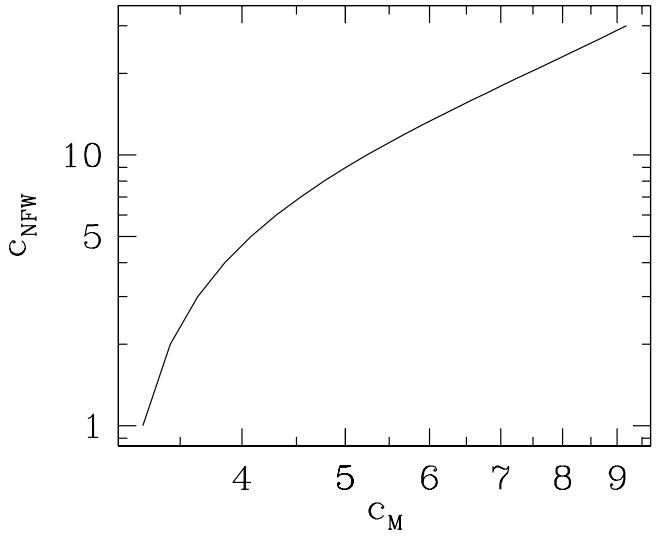

FIG. 6.—Mass concentration parameter c_M, defined in eq. (6), vs. NFW97 concentration parameter c_{NFW}.

where $x = r/r_{200}$, $v_c(x)$ is the circular velocity at x, and v_{200} is the circular velocity at r_{200}. Our v_{circ} is taken to be the maximum halo circular velocity, which may obtained by maximizing equation (8); this occurs at $x_{max} \approx 2/c_{NFW}$ (though we compute it exactly for the results shown below).

Let $\hat{v}_{circ} \equiv v_c(x_{max})/v_{200}$. In appropriate units, $v_{200} = r_{200}$ (see NFW97, their eq. [A2]). Thus,

$$x_{in} \equiv \frac{r_{in}}{r_{200}} = \frac{8.5}{220}\,\hat{v}_{circ}\,, \tag{9}$$

implying that x_{in} and $x_{out} = 3x_{in}$ are solely functions of c_{NFW} (note that this arises because we defined $r_{in} \propto v_{circ}$). Using $M(<r) \propto r v_c^2(r)$,

$$c_M = 9\,\frac{v_c^2(x_{in})}{v_c^2(x_{out})}\,, \tag{10}$$

which is purely a function of c_{NFW}. The resulting relationship is shown in Figure 6.

Figure 6 shows that $c_M \approx 8$, typical of halos in our CDM model, corresponds to $c_{NFW} \approx 23$. This value is in agreement with expectations for dwarf galaxies in a ΛCDM model. Conversely, $c_M \approx 5.6$, which is the median value for SIDM with 10^{-24} cm^2 GeV^{-1}, corresponds to $c_{NFW} \approx 11$. Note that the minimum value of c_M for an NFW97 halo is 3. Thus, SIDM with 10^{-23} cm^2 GeV^{-1}, with $c_{M,med} \sim 2.6$, produces halos that typically cannot be described properly by c_{NFW}. This is because these halos have $\alpha > -1$ typically, so NFW97 profiles with $\alpha(r \to 0) = -1$ are a poor fit.

The largest halo in our simulations has a mass comparable to that of the Milky Way, $\approx 6 \times 10^{11}\ M_\odot$. The concentrations of this halo are 6.7, 4.4, and 2.3 in CDM, $\sigma_{DM} = 10^{-24}$, and 10^{-23} cm^2 GeV^{-1}, respectively. The value of c_M of the Milky Way halo is somewhat uncertain because of the uncertainty in the rotation curve outside the solar circle ($R_\odot$) and the effect of baryonic mass within 1 $R_\odot$, but we make a rough estimate here. If the rotation curve is flat, $c_M = 9$ as stated before. There are suggestions that the rotation curve rises somewhat beyond the solar circle (though this is uncertain; see Olling & Merrifield 2000), in which case c_M is reduced; let us take $c_M = 8$ as a working estimate. The rotation curve measures the total mass, so we must correct for the baryons to compare with our simulated c_M. If we take the fraction of baryonic mass to be 50% inside 1 $R_\odot$ and 20% inside 3 $R_\odot$, then c_M reduces to 5. In addition, baryons adiabatically compress the dark matter as they dissipate, so we must correct the Milky Way c_M further downward to compare to our dissipationless halos. From the analysis of Avila-Reese, Firmani, & Hernandez (1998), this reduction factor is ~1.5–2, resulting in the Milky Way halo having $c_M \sim 3$. Thus, after reasonable corrections, the Milky Way mass concentration appears to be in better agreement with SIDM than CDM. The rapid rotation of bars also suggests a lower concentration for the Milky Way–sized galaxies than that predicted by CDM (Debattista & Sellwood 1998).

A more direct comparison with simulations may be obtained from rotation curves of dark matter–dominated, low surface brightness galaxies, where baryonic corrections are smaller. We expect that this mass concentration measure c_M will be relatively straightforward to compute from such rotation curves (e.g., Dalcanton & Bernstein 2000), so we look forward to comparisons. The mass concentration c_M has the advantage that it is independent of halo fitting parameters, as the enclosed mass can be obtained directly from the observed circular velocity with modest assumptions. In this sense, it is a more robust comparison than the inner slope and the NFW97 concentration parameter, which are degenerate and sensitive to scales outside those typically observed (van den Bosch & Swaters 2000), and the central density, which depends on an uncertain contribution from baryons.

3.6. *Phase Space Densities*

A recently popularized measure of the concentration of dark matter halos is the central phase space density. Dalcanton & Hogan (2000) find that observed phase space densities $Q \equiv \rho/\sigma^3$ scale as $Q \propto \sigma^{-3}$ to σ^{-4}, where σ is the

velocity dispersion, from dwarf spheroidals up to clusters of galaxies. Observations compiled by Sellwood (2000) suggest a similar relation, albeit with a large scatter, and he uses them to argue against any simple form of collisionless dark matter (though see Madsen 2000).

Figure 7 shows the phase space density Q of dark matter within $r_{\rm in}$ as a function of σ, for halos with $\sigma > 30$ km s^{-1}. We calculate σ as the velocity dispersion around the group center of mass velocity, within $r_{\rm in}$ (see eq. [7]). Open circles show CDM halos, while crosses indicate SIDM ($\sigma_{\rm DM} = 10^{-23}$ cm^2 GeV^{-1}) halos. The dashed and dotted lines show $Q \propto \sigma^{-3}$ and $Q \propto \sigma^{-4}$, respectively, which bracket the observations, reproduced from Dalcanton & Hogan (2000).

SIDM generally shows lower phase space densities than CDM. SIDM is in somewhat better agreement with observations, falling in the middle of the observed range. Measuring Q in galaxies is a difficult task because the stellar velocity dispersion is not necessarily that of the dark matter. Furthermore, in rotationally supported galaxies the dubious assumption of an isothermal spherical halo is used to relate circular velocity to dispersion. Thus, Q is perhaps not among the most useful observational discriminants between CDM and SIDM.

An interesting remark from Figure 7 is that the scaling of $Q(\sigma)$ is roughly the same in both models, approximately $Q \propto \sigma^{-3}$. Dalcanton & Hogan (2000) argue that such a scaling results from the dynamical assembly of halos and is not expected based on simple phase packing arguments. This further motivates simulations of SIDM that include the cosmological growth of halos via dynamical processes of merging and accretion.

3.7. *Ellipticities*

SIDM produces halos that are more spherical than CDM because of the isotropic nature of the collisions (Spergel & Steinhardt 2000). This is a generic feature of SIDM with *any* significant cross section, since in the inner portions of halos where collisions are frequent, the velocity ellipsoid is quickly isotropized. Thus, the shapes of dark matter halos provide an important observational discriminant between CDM and SIDM.

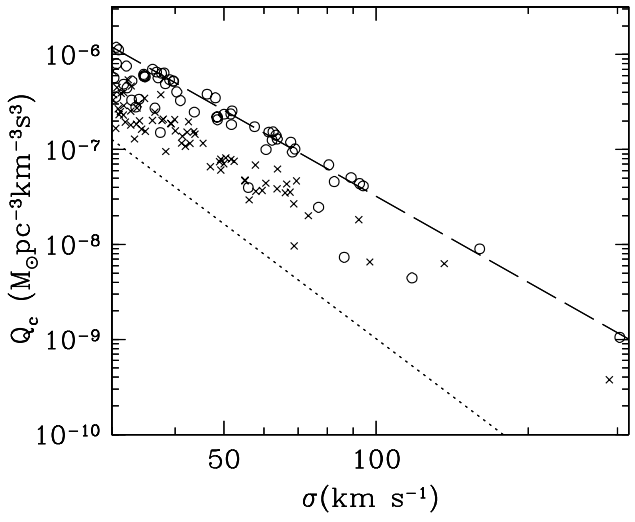

FIG. 7.—Phase space density Q vs. velocity dispersion σ for CDM (*open circles*) and SIDM with $\sigma_{\rm DM} = 10^{-23}$ cm^2 GeV^{-1} (*crosses*). Dashed and dotted lines bracket observations, showing scalings of $Q \propto \sigma^{-3}$ and $Q \propto \sigma^{-4}$, respectively.

We compute axis ratios of our halos using the prescription outlined in Dubinski & Carlberg (1991). They define a tensor

$$M_{ij} = \sum \frac{x_i x_j}{a^2} \quad \text{with } a \equiv \left(x_1^2 + \frac{x_2^2}{q^2} + \frac{x_3^2}{s^2} \right)^{1/2}, \qquad (11)$$

where a is the elliptical radius, $s \le q \le 1$ are the axis ratios, and the sum is over all particles with distances $\approx (x_1, x_2, x_3)$ from the halo center along the axes of the ellipsoid. Then,

$$q = \left(\frac{M_{yy}}{M_{xx}} \right)^{1/2},$$
$$s = \left(\frac{M_{zz}}{M_{xx}} \right)^{1/2}, \qquad (12)$$

where $M_{xx} \ge M_{yy} \ge M_{zz}$ are the eigenvalues of M, q represents the axisymmetry of the halo, and s measures the halo flattening. Since a depends on q and s, the calculation of M_{ij} must be iterated until convergence, which we take to be better than 0.01 in q and s. This scheme weights particles roughly equally regardless of distance from center, unlike a moment-of-inertia tensor that weights the outskirts heavily, and thus better represents the ellipticity of the density distribution, as shown in Dubinski & Carlberg (1991).

Figure 8 shows axis ratios as a function of radius in our two most massive halos, having masses $\approx 6 \times 10^{11}\ M_\odot$ (*left panel*) and $\approx 7 \times 10^{10}\ M_\odot$ (*right panel*). The solid line is the CDM halo, dashed line is SIDM with $\sigma_{\rm DM} = 10^{-24}$ cm^2 GeV^{-1}, and dot-dashed line is SIDM with $\sigma_{\rm DM} = 10^{-23}$ cm^2 GeV^{-1}; q is the upper of two curves for a given model.

CDM halos are fairly triaxial, while SIDM produces halos that are much closer to spherical. The effect is dependent on radius, as in the outer regions SIDM and CDM become more similar, since the effect of self-interactions is confined to the inner parts of halos. Still, even at 30 h^{-1} kpc there are significant differences between SIDM and CDM. While not stated, this trend with radius is also evident from Figure 1 of Yoshida et al. (2000b).

Figure 9 shows histograms of axis ratios q and s at 2 h^{-1} kpc (*top panels*) and 10 h^{-1} kpc (*bottom panels*) for all halos with more than 1000 particles. The median value for each model is indicated by the corresponding tick mark on the top axis. The difference between CDM and SIDM is more pronounced at small radii, where CDM produces significantly triaxial halos while SIDM halos remain spherical. At large radii there is a much milder trend to more spherical halos with increasing $\sigma_{\rm DM}$; s also shows more differences than q.

Figure 9 shows that while CDM produces halos that are typically more spherical, there is still significant nonsphericity in many SIDM halos. In particular, there is a tail in the distributions of both CDM and SIDM to smaller axis ratios. This may be due to asymmetric infall that temporarily distorts the shape of the density in some halos, particularly smaller ones. This also may just be an artifact of a finite number of collisions in smaller halos. Note that the two largest halos shown in Figure 8 show greater differences at 10 h^{-1} kpc than suggested by the statistics in Figure 9.

A comparison with observations of halo shapes is as yet inconclusive. In the inner portions of dark halos the shape

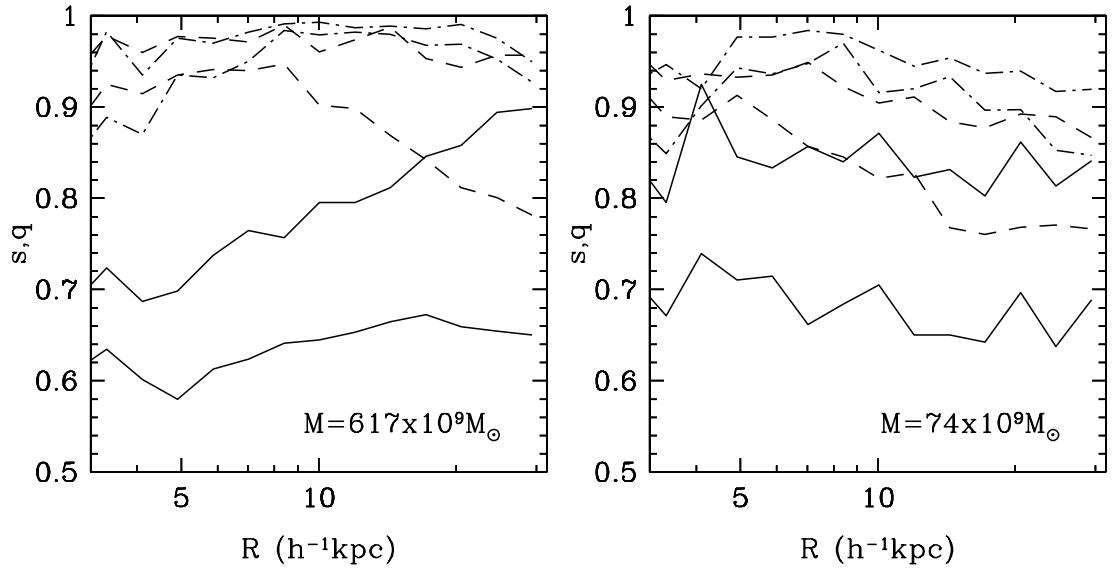

FIG. 8.—Axisymmetry q and flattening s vs. r for a $6 \times 10^{11}\ M_\odot$ halo (*left panel*) and a $7 \times 10^{10}\ M_\odot$ halo (*right panel*). Solid lines are CDM; dashed lines are SIDM, $\sigma_{\rm DM} = 10^{-24}$ cm^2 GeV^{-1}; and dot-dashed lines are SIDM, $\sigma_{\rm DM} = 10^{-23}$ cm^2 GeV^{-1}. Lower of two curves is s.

of the potential is likely to be dominated by baryons, so a comparison to these simulations is not straightforward. Farther out, perhaps the most direct observations of axisymmetry are those for galaxies with H I rings such as IC 2006, which suggests a very axisymmetric halo, $q \approx 0.93 \pm 0.08$ at $\approx$13 kpc (Franx, van Gorkom, & de Zeeuw 1994). Other observations (see Sackett 1999) are more dependent on observational and theoretical uncertainties such as viewing angle and potential modeling but persistently suggest $q \gtrsim 0.8$ at $\sim$15–20 kpc. Both CDM and SIDM halos are consistent with these observations. Lensing maps of galaxies and clusters offer the best hope for mapping the mass potential in the inner halos, which should place strong constraints on SIDM.

Conversely, observations of s from polar ring galaxies (e.g., Sackett et al. 1994) and X-ray isophotes (e.g., Buote & Canizares 1998) suggest a substantial amount of flattening, $s \approx 0.5 \pm 0.2$ at $r \sim 15$ kpc, in the density distribution. Such a flattening, if confirmed, may prove troublesome for SIDM. The baryonic component would provide a flattened contribution but is not expected to be significant at those radii. It is not immediately evident how these discrepancies may be resolved, but we note that the problem is almost as severe for CDM as for SIDM in our simulations. It is worth mentioning that our small simulation volume results in significantly reduced tidal distortion of large halos, so our simulations may not accurately represent the ellipticities of the outer portions of halos.

4. THE MONTE CARLO RESOLUTION LIMIT

Our spatial resolution and mass resolution are well understood. However, another resolution issue arises because of the Monte Carlo modeling of self-interactions. A Monte Carlo method must be sufficiently well sampled, resulting in a separate criterion for the number of particles in a halo to be well represented by our simulation technique. In this section we determine this criterion using our suite of lower resolution simulations with 64^3 particles described in § 2.

Since we are most concerned with the inner parts of halos, we focus on the inner slope as a function of mass as the best measure for examining this Monte Carlo resolution limit. Figure 10 shows a plot similar to the right panel of Figure 4, except for the 64^3 simulation of the $\sigma_{\rm DM} = 10^{-23}$ cm^2 GeV^{-1} SIDM model. The top axis shows the number of particles in these halos. Here we compute α at $2\ h^{-1}$ kpc since that is the spatial resolution of our 64^3 runs. The dashed line is the running median α from the 128^3 simulation, computed at $2\ h^{-1}$ kpc.

Figure 10 shows that for halos with $\gtrsim$1000 particles in the 64^3 run, the median value of α is within 1 σ of that of the 128^3 run, though consistently lower. By 300 particles, the value of α is significantly lower in the 64^3 run. The reason it is lower is because with few particles, the Monte Carlo procedure results in too few interactions to make the profile depart significantly from the collisionless CDM case. Thus, to lower masses, SIDM looks increasingly like CDM when modeled using this technique.

Note that this limit is specific to our simulation parameters, redshift, and $\sigma_{\rm DM}$ and is not a general statement about the Monte Carlo N-body technique. The limit becomes higher as $\sigma_{\rm DM}$ is lowered, since collisions become less frequent, but even for $\sigma_{\rm DM} = 10^{-24}$ cm^2 GeV^{-1}, 1000 or more particle halos also appear convergent. We therefore take our Monte Carlo resolution limit to be $\gtrsim$1000 particles.

We list the values of $\alpha_{\rm med}$ and $c_{M,\rm med}$ for the 64^3 runs in Table 1 for comparison with the 128^3 results, where the median values here are computed for all halos with more than 500 particles in these smaller runs (roughly 10 in each simulation). Note that $\alpha_{\rm med}$ is computed at $2\ h^{-1}$ kpc instead of $1\ h^{-1}$ kpc, partially explaining the steeper slopes even at the highest masses. In general, the trends indicated by the 128^3 runs are reproduced at this lower resolution, suggesting that discrete particle effects do not significantly affect our conclusions. We have also examined the 128^3 statistics presented previously using a limit of 300 particles instead of 1000, and our overall conclusions remain the same.

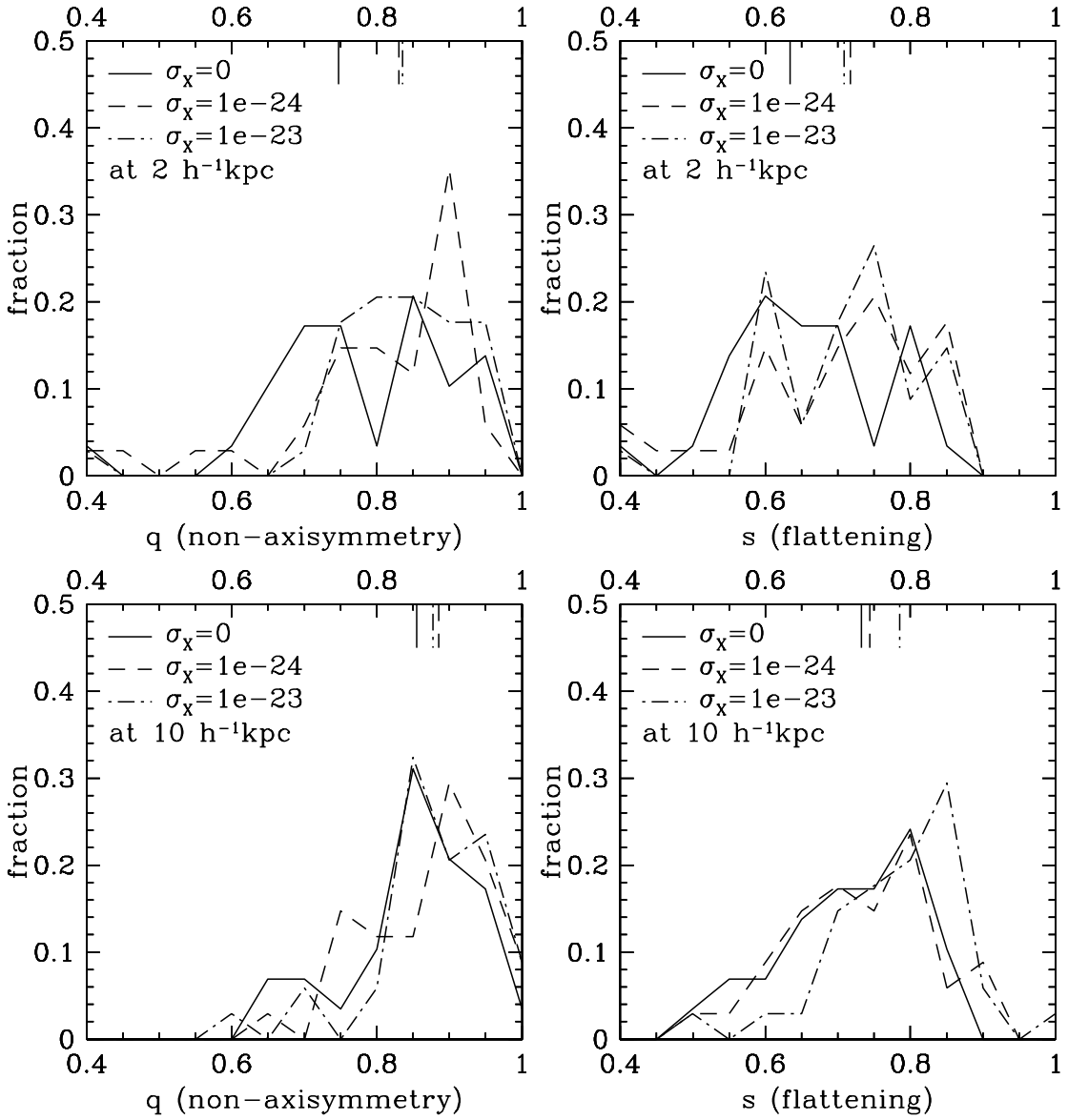

FIG. 9.—Histogram of axis ratios q (*left panels*) and s (*right panels*), at 2 h^{-1} kpc (*upper panels*) and 10 h^{-1} kpc (*lower panels*). Only halos with more than 1000 particles are included. Tick marks at the upper axis show median values.

5. SUBHALO POPULATION

Self-interacting dark matter is predicted to lower significantly the population of subhalos orbiting around large halos, thereby bringing simulation predictions into better agreement with observations of the Local Group dwarf population. There are two reasons why SIDM has this effect: (1) the lowered central concentration and larger core radius make small halos more susceptible to tidal disruption and (2) dark matter is ram pressure stripped out of small galaxies as they move through the large central halo. In our 128^3 simulations, we have one halo that is roughly Milky Way sized, having $M \approx 6.7 \times 10^{11}\ M_\odot$. In this section we examine the subhalo population around this large halo.

Figure 11 shows a projected plot of halos within 500 h^{-1} kpc of the largest halo in our volume, indicated by the central cross. Circle sizes are scaled as log ($M_{\rm halo}$), with the smallest circles representing halos with $M \approx 5 \times 10^8\ M_\odot$. The left panel shows CDM, while the right panel shows SIDM with $\sigma_{\rm DM} = 10^{-23}$ cm^2 GeV^{-1}. The positions of subhalos are different because of the accumulated differences of chaotic orbits within a highly nonlinear potential well. Thus, a halo-by-halo comparison for these small halos is not possible. A careful examination reveals that SIDM has fewer subhalos than the CDM distribution, especially the smallest ones.

Figure 12 quantifies this effect, showing the mass function of halos within 500 h^{-1} kpc of our largest halo, for our three 128^3 simulations. There is a clear trend that SIDM suppresses the subhalo population at the smallest masses. For $10^{8.5} < M < 10^9\ M_\odot$, CDM has 56 neighboring halos, $\sigma_{\rm DM} = 10^{-24}$ cm^2 GeV^{-1} has 40, and $\sigma_{\rm DM} = 10^{-23}$ cm^2 GeV^{-1} has 29.

While SIDM does reduce the population of smallest halos, the reduction is not nearly by the order of magnitude required to obtain agreement with Local Group dwarf galaxy counts (Moore et al. 1999a). However, the effect of subhalo suppression in these SIDM simulations should be

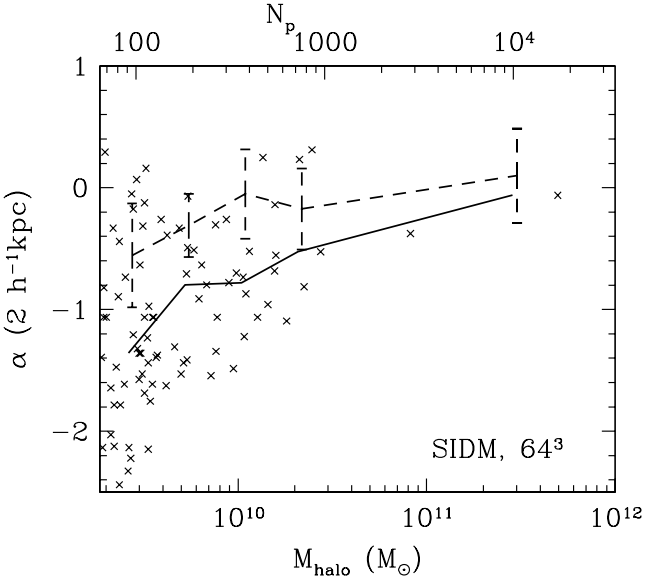

FIG. 10.—α vs. $M_{\rm halo}$ for SIDM with $\sigma_{\rm DM} = 10^{-23}$ cm^2 GeV^{-1}, for our 64^3 run. Here α is measured at 2 h^{-1} kpc, the resolution of our 64^3 runs. The solid line shows a running median of the α distribution. The dashed line with error bars shows a similar curve from 128^3 run. Deviations between the two at a level greater than 1 σ occur for halos having somewhere between 300 and 1000 particles.

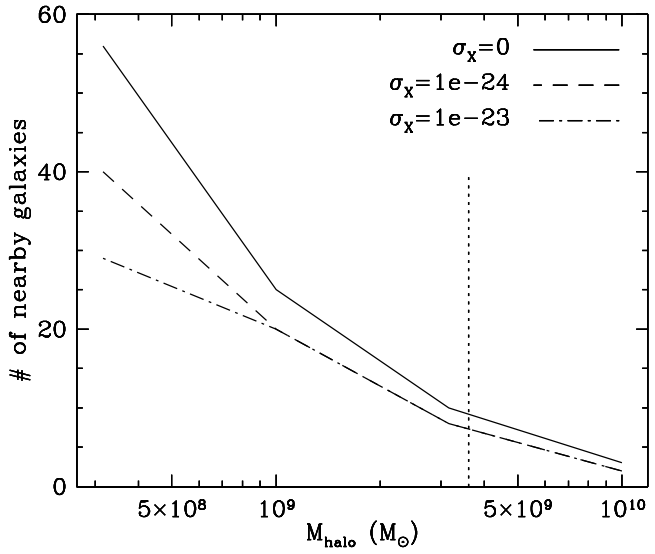

FIG. 12.—Number of halos within 500 h^{-1} kpc of the largest halo, histogrammed by mass, for collisionless (*solid line*), 10^{-24} cm^2 GeV^{-1} (*dashed line*), and 10^{-23} cm^2 GeV^{-1} (*dot-dashed line*). Vertical dotted line indicates our 1000 particle Monte Carlo resolution limit.

regarded as a lower limit to the true strength of the effect. The reason is that almost all these subhalos are well below our Monte Carlo resolution limit (*dotted line* in Fig. 12); therefore, their concentrations are approaching those in CDM models. Thus, tidal disruption of these halos is not much stronger in SIDM than in CDM and is increasingly similar to lower masses. Furthermore, ram pressure stripping is reduced in effectiveness for the same reason that the Monte Carlo technique is less effective in these small halos. Hence, the numbers of small SIDM halos are not as significantly suppressed relative to CDM as they should be.

We conclude that the simulations considered here suggest a weak trend in reducing the number of subhalos with increasing $\sigma_{\rm DM}$, but because of resolution effects we can make no robust quantitative estimates. What is required is to simulate a large halo with incredibly high resolution, having subhalos containing thousands of particles to model the effects of self-interactions properly. Such a simulation is unfortunately beyond the scope of our current computational resources. Alternatively, more sophisticated algorithms are necessary to model self-interactions in small halos moving through large ones, which is an avenue we are currently pursuing.

6. COMPARISON WITH PREVIOUS WORK

A number of authors have investigated SIDM using N-body simulations. The literature divides into two subsets:

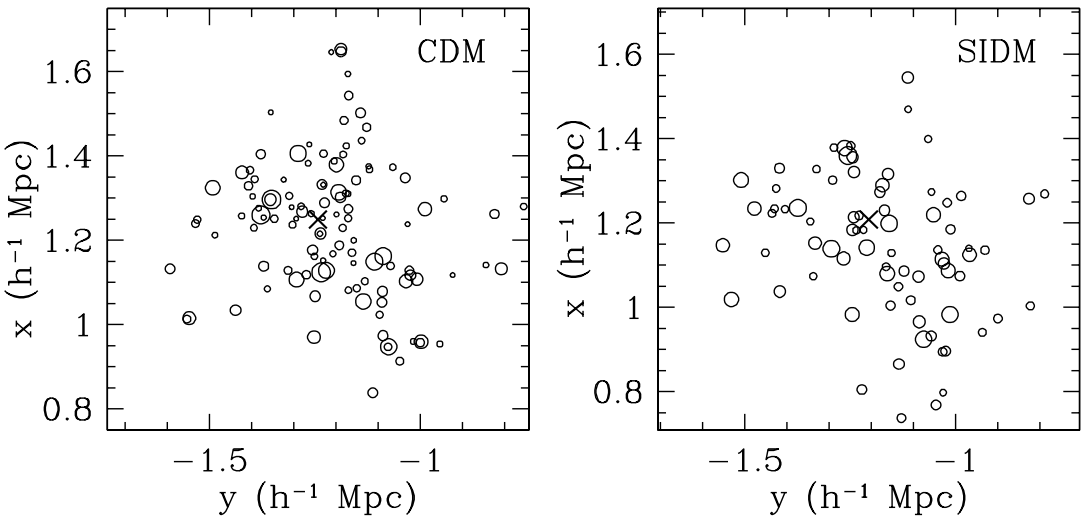

FIG. 11.—Subhalo positions within 500 h^{-1} kpc, the largest object in our volume, in CDM (*left panel*) and SIDM with $\sigma_{\rm DM} = 10^{-23}$ cm^2 GeV^{-1} (*right panel*). Central cross is the position of the large halo.

those that model interactions in the fluid approximation, effectively employing a large cross section, and those that model self-interactions in the optically thin regime as suggested by Spergel & Steinhardt (2000). In both cases, there is disagreement over whether SIDM makes halos less or more concentrated than CDM.

Moore et al. (2000) and Yoshida et al. (2000a) simulate a galaxy cluster within a cosmological context, using a tree code with SPH to model interactions in the fluid approximation. Both studies resulted in halos that had isothermal profiles and were more centrally concentrated than CDM halos. This may be because the large effective cross section increases heat transfer efficiency, though as mentioned in § 1, for a sufficiently large cross section one expects heat transfer to be diminished. Yoshida et al. (2000a) suggested that intermediate cross sections would likely yield results that were intermediate between steep CDM profiles and steeper isothermal profiles and thereby argued against SIDM. However, this is contradicted by Yoshida et al. (2000b), as well as by the results presented here, confirming that the intermediate case results in halos that have long-lived shallow profiles.

In contrast, G. Bryan (2000, private communication) uses an adaptive mesh hydrodynamics code to model self-interactions in a cosmological volume and finds that even in the fluid limit SIDM produces sizeable, long-lived cores. U.-L. Pen (2000, private communication) finds the same using a moving mesh code, which may be a clue that the issue is mesh versus particles, not Eulerian versus Lagrangian. However, it is not clear why different hydrodynamic codes give different results when they should be operating in the same regime. Perhaps the effective cross section is larger in the adaptive mesh code as a result of algorithmic differences, reducing heat transfer. Another possibility is that a numerical effect in SPH in which cold clumps moving through hot halos have their drag significantly overestimated (Tittley, Couchman, & Pearce 1999) makes objects rapidly sink into a dense, isothermal core. It is beyond the scope of this paper to resolve these issues. We simply note that the highly optically thick limit is not the relevant scenario to test the cross section range proposed by Spergel & Steinhardt (2000).

Burkert (2000) and Kochanek & White (2000) simulated isolated halos with SIDM having a cross section closer to the range of Spergel & Steinhardt (2000). They begin with a fully formed cuspy galaxy halo and study the evolution after interactions are turned on. They both find that halos develop a shallow core for some length of time and then undergo core collapse. Burkert (2000) and Kochanek & White (2000) disagree on the timescales of core collapse; Burkert (2000) finds $t_c \sim 16 t_{\rm dyn}$ in agreement with estimates from two-body relaxation, while Kochanek & White (2000) finds a much shorter collapse timescale of $t_c \sim 2 t_{\rm dyn}$ for the same dark matter cross section. Kochanek & White (2000) explain this difference by arguing that the Burkert (2000) method underestimates collisions of slow-moving particles. We note that our method does not suffer from this concern, as it is more like Kochanek & White (2000).

We suggest some possible reasons why the results of Kochanek & White (2000) and (to a lesser extent) Burkert (2000) are at odds with ours. The first is that they begin with a cuspy Hernquist profile. This halo evolves rapidly initially (as seen in Fig. 3 of Kochanek & White 2000), resulting in an artificially large amount of heat transfer. Second, they simulate an isolated halo, ignoring the accretion of dynamically hot material during the formation process that would keep the outer halo hot and delay core collapse. We note that their dimensionless cross section $\hat{\sigma}_{\rm DM} = M_{\rm halo}\sigma_{\rm DM}/r_s^2$ converts to ours by a factor of $\sim 2 \times 10^{-23}$ cm^2 GeV^{-1} for $M_{\rm halo} \approx 2 \times 10^{10}\ M_\odot$ and $r_s \approx 5\ h^{-1}$ kpc (see Fig. 1). The Kochanek & White (2000) simulation with $\hat{\sigma}_{\rm DM} = 1$ already produces halos that maintain cores over many dynamical times (see *top panel* of their Fig. 2). We suggest that a somewhat smaller $\hat{\sigma}_{\rm DM}$ might be consistent with observations as well as their limits on core collapse timescales, even without considering the effects of accretion and merging.

Kochanek & White (2000) also point out, as we have, that the Monte Carlo N-body technique requires a large number of particles for accurate modeling and show that 10^5 particles are sufficient. We note that while most of our halos do not have that many particles, our largest (Milky Way–sized) halo has roughly 2×10^5 particles, and its properties are consistent with those of smaller halos.

Yoshida et al. (2000b) have now performed a cosmological cluster simulation with cross sections $\sigma_{\rm DM} \approx 2 \times 10^{-25}$ to 2×10^{-23} cm^2 GeV^{-1} using a Monte Carlo N-body method. They find shallower central slopes and less concentrated cores with SIDM. Our combined results span the range from dwarf galaxies to clusters and are in broad agreement with each other using simple scaling arguments detailed in their paper. As they point out, the cross sections that our simulations favor for consistency with dwarf galaxy properties may produce cluster cores that are too large when compared with observations; we will discuss this further in the next section.

In order to explore the high-$\sigma_{\rm DM}$ limit, we ran 64^3 simulations of SIDM with $\sigma_{\rm DM} = 10^{-25}$ to 10^{-22} cm^2 GeV^{-1}. The most illustrative result is to compare the density profile of the largest halo in all our 64^3 simulations, as shown in Figure 13. As seen in Figure 1, there is a smooth trend of increasing core radius with $\sigma_{\rm DM}$. SIDM with $\sigma_{\rm DM} = 10^{-25}$ cm^2 GeV^{-1} is quite similar to CDM, though it may also have a core below our $2\ h^{-1}$ kpc resolution limit. Increasing $\sigma_{\rm DM}$ to 10^{-22} cm^2 GeV^{-1}, we continue to see no evidence

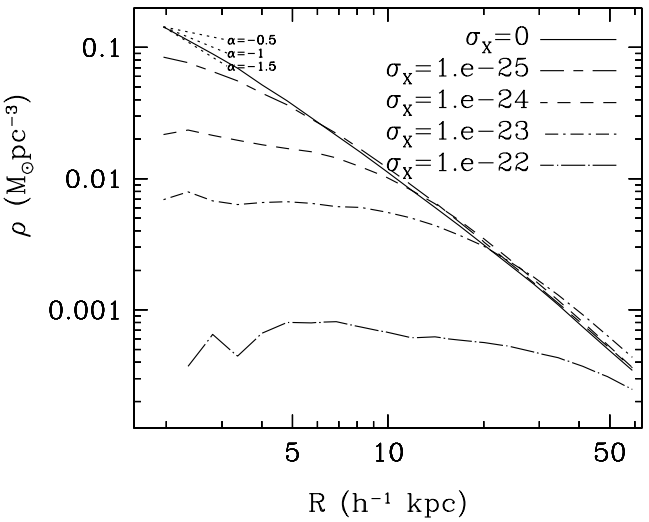

FIG. 13.—Halo profile of the largest halo in our 64^3 simulations, for a range of $\sigma_{\rm DM}$ values. Halos are progressively less concentrated and have larger cores with increasing $\sigma_{\rm DM}$.

for the development of an isothermal core due to accelerated heat transfer. The reason is because the collisions are so frequent in the outer portion of the halo that a dense core cannot develop. Instead, collisions randomize the dark matter velocities and prevent a smooth radial inflow required to generate a dense core. As dynamically hot material accretes onto the halo, heat keeps flowing inward and a large core is maintained. This illustrates why simulating SIDM beginning with an isolated cuspy Hernquist profile may not be appropriate for large $\sigma_{\rm DM}$; one should at least begin with a halo profile that is self-consistently stable for a few dynamic times. While we are not likely to be approaching the fluid limit even at $\sigma_{\rm DM} = 10^{-22}$ cm^2 GeV^{-1}, the trend in our results is in better agreement with Bryan as opposed to Moore et al. (2000) and Yoshida et al. (2000a).

7. SUMMARY

We present a set of cosmological self-interacting dark matter simulations having cross sections in the range favored by Spergel & Steinhardt (2000). Our simulations include the growth of halos from linear fluctuations in a random volume of the universe, with sufficient volume and resolution to obtain a statistical sample of galactic halos resolved to 1 h^{-1} kpc. We compare the resulting halos on a case-by-case basis to those in a collisionless CDM simulation having the same initial conditions.

Overall, SIDM is remarkably successful at reproducing observations of the inner portions of dark matter halos where CDM appears to fail. In particular, we find the following:

1. The inner slopes of SIDM with $\sigma_{\rm DM} = 10^{-23}$ cm^2 GeV^{-1} typical halos have $\alpha \approx -0.4$ at $r \sim 1$ h^{-1} kpc, with some scatter in α. Our CDM halos have $\alpha \approx -1.5$, in agreement with previous studies, though since we cannot measure the asymptotic inner slope, we cannot distinguish between a Moore et al. (1999b) profile and an NFW97 profile. SIDM with $\sigma_{\rm DM} = 10^{-24}$ cm^2 GeV^{-1} is intermediate between these cases, with median $\alpha \approx -0.9$. SIDM is in better agreement with a preliminary analysis of Hα rotation curves of low surface brightness galaxies (Dalcanton & Bernstein 2000).

2. SIDM with $\sigma_{\rm DM} = 10^{-23}$ cm^2 GeV^{-1} produces central densities $\rho_c \sim 0.01\ M_\odot$ pc^{-3} at 1 h^{-1} kpc and shows no trend with halo mass. SIDM with $\sigma_{\rm DM} = 10^{-24}$ cm^2 GeV^{-1} has somewhat higher ρ_c values but remains fairly independent of mass. Conversely, ρ_c in CDM halos is much larger than observed, typically $\gtrsim 0.1\ M_\odot$ pc^{-3} at 1 h^{-1} kpc, and shows a strong trend with halo mass. With their steep profiles, CDM halos are in significantly worse agreement at smaller radii. SIDM is thus in better agreement with observations, as has also been argued by Firmani et al. (2000a).

3. Simulations with SIDM having $\sigma_{\rm DM} = 10^{-24}$ cm^2 GeV^{-1} are intermediate between CDM and SIDM with $\sigma_{\rm DM} = 10^{-23}$ cm^2 GeV^{-1}, indicating a smooth increase in the effect of SIDM with cross section, a result that extends (using lower resolution simulations) from $\sigma_{\rm DM} = 10^{-25}$ to 10^{-22} cm^2 GeV^{-1}. In particular, the generation of singular isothermal halos is not seen in any of the massive halos simulated, even for $\sigma_{\rm DM} = 10^{-22}$ cm^2 GeV^{-1}. This suggests that the dynamical process of halo growth in a cosmological setting helps keep outer regions of halos hot and prevents core collapse in a Hubble time.

4. We introduce a new mass concentration parameter c_M based on a more directly observable quantity, the enclosed mass within tens of kiloparsecs. This halo concentration is significantly lower in SIDM models as compared to CDM, providing an observationally accessible discriminant that is not dependent on fitting a particular profile form. A rough estimate of c_M for the Milky Way, with large corrections for baryonic effects, favors SIDM over CDM.

5. The central phase space density is lower in SIDM versus CDM mostly because of the reduction in ρ_c. The velocity dispersions in the inner regions are quite similar. Both SIDM and CDM are consistent with observations shown in Dalcanton & Hogan (2000), though SIDM is mildly favored.

6. SIDM produces halos that are more spherical, especially in their inner regions, as compared to CDM. In principle, this is one of the strongest tests of the SIDM paradigm, as near the center *any* value of $\sigma_{\rm DM}$ that has a nonnegligible effect on the dark matter distribution will increase the core sphericity, while CDM cores are almost always significantly triaxial. However, baryons are likely to dominate the shapes of the inner parts of halos, complicating a direct comparison, and in the outer parts the differences between SIDM and CDM are less pronounced.

7. The number of subhalos around our largest (Milky Way–sized) halo is somewhat reduced with increasing $\sigma_{\rm DM}$, but because of discreteness effects in our Monte Carlo N-body technique, we cannot put robust quantitative estimates on the strength of this effect.

Based on these simulations, our currently favored value for $\sigma_{\rm DM}$ is somewhere between 10^{-23} and 10^{-25} cm^2 GeV^{-1}. While our statistics favor closer to the upper range, because of our limited resolution and discreteness effects in our Monte Carlo technique, we cannot firmly rule out the lower end of that range as being consistent with dwarf galaxy properties. SIDM produces better agreement with observations for both the observed central density and inner profile slope, which is nontrivial. In contrast, for instance, warm dark matter has difficulty simultaneously reproducing the observed central densities, inner slopes, and subhalo population (Colín et al. 2000).

As stated before, inner halo shapes may provide a strong discriminant between CDM and SIDM. On galactic scales, they are difficult to observe and are confused by baryonic contributions. Conversely, clusters provide a cleaner test because they have large cores that are not baryon dominated, and their mass distributions are directly observable via lensing. Miralda-Escudé (2000) uses the asphericity of cluster MS 2137−23 to argue (analytically) that $\sigma_{\rm DM} < 10^{-25.5}$ cm^2 GeV^{-1}, effectively ruling out SIDM as a solution to halo concentration problems. On the other hand, CL 0024+1654 is very spherical, much more so than CDM models generally predict (Tyson et al. 1998). Our simulations cannot directly address the shapes of clusters, as we have no cluster-sized objects in our volume. However, SIDM shows some range of halo shapes due to asymmetric infall and unrelaxed mass distributions, so it is unclear whether a single object can definitively rule out SIDM. Support for this statement is provided by Yoshida et al. (2000b), whose cluster has enough triaxiality to be consistent with MS 2137−23 even for $\sigma_{\rm DM} \approx 2 \times 10^{-24}$ cm^2 GeV^{-1} (their model S1Wb), contradicting Miralda-

Escudé's (2000) scaling argument. We note that halo shapes are unaffected by annihilating (Kaplinghat et al. 2000) or decaying (Cen 2000) dark matter, thus they also provide a discriminant between these variants and SIDM.

The core size in the 10^{15} $M_\odot$ cluster simulation of Yoshida et al. (2000b) is larger than observed ($\sim$30–70 h^{-1} kpc; Miralda-Escudé 1995; Tyson et al. 1998), certainly for $\sigma_{\rm DM} \approx 2 \times 10^{-23}$ cm^2 GeV^{-1} (160 h^{-1} kpc), and probably even for $\sigma_{\rm DM} \approx 2 \times 10^{-24}$ cm^2 GeV^{-1} (100 h^{-1} kpc). While they only simulated a single cluster, we have now run simulations with larger volume that suggest that their results are typical for clusters of that size. So we may be forced toward the lower end of our cross section range by cluster core sizes, if we insist on a velocity-independent cross section. Note that adiabatic contraction of baryons during the formation of the cD galaxy will reduce the cluster core radius from N-body predictions, so the discrepancy may not be that large. In any case, SIDM with $\sigma_{\rm DM} \approx 10^{-25}$ to 10^{-23} cm^2 GeV^{-1} comes fairly close to matching dwarf galaxies, L_* galaxies, and clusters given the $\sim 10^5$ range in mass scales, so we reserve judgment pending improved simulations and a more careful comparison with observations. Yoshida et al. (2000b) mention that SIDM cluster core sizes would be in better agreement with observations if $\sigma_{\rm DM} \propto v^{-1}$, which would result in the effects of self-interactions being diminished in hot cluster environments as compared to galaxies. While our analysis does not yet require this, it may alleviate the tightness of some constraints. Such a scenario occurs naturally if the dark matter–dark matter scattering has low-lying resonance or bound-state contributions, as is the case for ordinary nucleons.

Strong lensing by clusters also provides a constraint on SIDM, since a lower central density results in many fewer multiple images. This avenue was explored by Wyithe, Turner, & Spergel (2000), who find that $\sigma_{\rm DM} \approx 2 \times 10^{-23}$ produces 1–2 orders of magnitude fewer multiply imaged sources than in the CDM case. In principle this is a strong discriminant. However, if there is a greater spread in halo profiles in SIDM versus CDM, as is predicted by our simulations, the discrimination may be reduced since lensing statistics will be dominated by the most concentrated objects.

Various theoretical avenues have been explored in relation to SIDM. For instance, Mo & Mao (2000) determine that a cross section of $\sigma_{\rm DM} \sim 10^{-23}$ cm^2 GeV^{-1} would produce a correct Tully-Fisher relation for $v_{\rm circ} \approx 100$ km s^{-1} halos. Thus, it is conceivable that the cross section preferred from halo structure constraints may also alleviate the Tully-Fisher discrepancies. Another example is provided by Ostriker (2000), who argues that dark matter interactions arising from $\sigma_{\rm DM} \sim 10^{-24}$ cm^2 GeV^{-1} would naturally generate central black holes with masses $M_{\rm BH} \propto \sigma^{4.5}$ (where σ is the halo velocity dispersion), in agreement with observations (Ferrarese & Merritt 2000), as well as roughly the correct mass.

Observations of dark matter halos promise to improve significantly in the coming years, particularly constraints on halo core shapes from lensing and on inner profiles and concentrations of halos from Hα rotation curves. If the inner parts of dark matter halos are found to be generically triaxial, this would be the high place of sacrifice for self-interacting dark matter; conversely, spherical halos would provide strong support for this scenario. The main modeling work yet to be done is an improved examination of the subhalo populations in SIDM, as well as simulations of a larger range of mass scales. The N-body Monte Carlo approach has difficulty achieving a large dynamic range because of the stringent Monte Carlo resolution limit (i.e., discreteness effects in the probabilistic description of collisions); therefore, a different approach may be necessary.

The SIDM simulations presented here are a first attempt at examining the effect of self-interacting dark matter within the context of a realistic halo formation scenario. The results are encouraging that this simple variant of the cold dark matter paradigm will alleviate a wide range of difficulties faced by CDM on galactic scales. We look forward to further investigations and comparisons with observations.

We thank Julianne Dalcanton, Lars Hernquist, Jerry Ostriker, Penny Sackett, Scott Tremaine, Martin White, and Naoki Yoshida for helpful discussions. We thank Greg Bryan and Ue-Li Pen for sharing their unpublished results. We thank Volker Springel for the use of his GADGET code. R. D. and D. N. S. are supported by NASA ATP grant NAG5-7066. D. N. S. and B. D. W. are supported by the NASA MAP/MIDEX program. P. J. S. is supported by US Department of Energy grant DE-FG02-91ER40671.

REFERENCES

Avila-Reese, V., Firmani, C., & Hernandez, X. 1998, ApJ, 505, 37
Bahcall, N., Ostriker, J. P., Perlmutter, S., & Steinhardt, P. J. 1999, Science, 284, 1481
Bento, M. C., Bertolami, O., Rosenfeld, R., & Teodoro, L. 2000, Phys. Rev. D., 62, 1
Blitz, L., Spergel, D. N., Teuben, P. J., Hartmann, D., & Burton, W. B. 1999, ApJ, 514, 818
Bullock, J. S., Kravtsov, A. V., & Weinberg, D. H. 2000, ApJ, 539, 517
Buote, D. A., & Canizares, C. R. 1998, MNRAS, 298, 811
Burkert, A. 2000, ApJ, 534, L143
Caldwell, R. R., Dave, R., & Steinhardt, P. J. 1998, Phys. Rev. Lett., 80, 1582
Cen, R. 2000, ApJ, submitted
Colín, P., Avila-Reese, V., & Valenzuela, O. 2000, ApJ, 542, 622
Dalcanton, J. J., & Bernstein, R. A. 2000, in 25th IAP Meeting, Dynamics of Galaxies: From the Early Universe to the Present, ed. F. Combes, G. A. Mamon, & V. Charmandaris (Paris: Editions Frontieres), 161
Dalcanton, J. J., & Hogan, C. J. 2000, ApJ, submitted (astro-ph/0004381)
Debattista, V. P., & Sellwood, J. A. 1998, ApJ, 493, L5
de Blok, W. J. G., McGaugh, S. S., & van der Hulst, J. M. 1996, MNRAS, 283, 18
Dubinski, J., & Carlberg, R. G. 1991, ApJ, 378, 496
Ferrarese, L., & Merritt, D. 2000, ApJ, 539, L9
Firmani, C., D'Onghia, E., Avila-Reese, V., Chincarini, G., & Hernandez, X. 2000a, MNRAS, 315, 29
Firmani, C., D'Onghia, E., Chincarini, G., Hernandez, X., & Avila-Reese, V. 2000b, MNRAS, submitted (astro-ph/0005001)
Franx, M., van Gorkom, J. M., & de Zeeuw, T. 1994, ApJ, 436, 642
Goodman, J. 2000, NewA, 5, 103
Hannestad, S., & Scherrer, R. J. 2000, Phys. Rev. D, 62, 043522
Hernquist, L. 1990, ApJ, 356, 359
Hu, W., Barkana, R., & Gruzinov, A. 2000, Phys. Rev. Lett., 85, 1158
Jing, Y. P., & Suto, Y. 2000, ApJ, 529, L69
Kaplinghat, M., Knox, L., & Turner, M. 2000, Phys. Rev. Lett., 85, 3335
Katz, N., Weinberg, D. H., & Hernquist, L. 1996, ApJS, 105, 19
Klypin, A. 2000, Relativistic Cosmology: Theory and Observations (astro-ph/0005504)
Klypin, A., Kravtsov, A. V., Valenzuela, O., & Prada, F. 1999, ApJ, 522, 82
Kochanek, C. S., & White, M. 2000, ApJ, 543, 514
Kravtsov, A. V., Klypin, A., Bullock, J. S., & Primack, J. P. 1998, ApJ, 502, 48
Ma, C.-P., & Bertschinger, E. 1995, ApJ, 455, 7
Madsen, J. 2000, Phys. Rev. Lett., submitted (astro-ph/0006074)
Miralda-Escudé, J. 1995, ApJ, 438, 514
———. 2000, ApJ, submitted (astro-ph/0002050)
Mo, H. J., & Mao, S. 2000, MNRAS, 318, 163

Moore, B., Gelato, S., Jenkins, A., Pearce, F. R., & Quilis, V. 2000, ApJ, 535, L21
Moore, B., Ghigna, S., Governato, F., Lake, G., Quinn, T., Stadel, J., & Tozzi, P. 1999a, ApJ, 524, L19
Moore, B., Quinn, T., Governato, F., Stadel, J., & Lake, G. 1999b, MNRAS, 310, 1147
Narayanan, V., Spergel, D. N., Davé, R., & Ma, C.-P. 2000, ApJ, 543, L103
Navarro, J. F., Frenk, C. S., & White, S. D. M. 1997, ApJ, 490, 493 (NFW97)
Navarro, J. F., & Steinmetz, M. 2000, ApJ, 528, 607
Olling, R. P., & Merrifield, M. R. 2000, MNRAS, 311, 361
Ostriker, J. P. 2000, Phys. Rev. Lett., 84, 5258
Peebles, P. J. E. 2000, ApJ, 534, L127
Riotto, A., & Tkachev, I. 2000 (astro-ph/0003388)
Sackett, P. D. 1999, in ASP Conf. Ser. 182, Galaxy Dynamics, ed. D. Merritt, J. A. Sellwood, & M. Valluri (San Francisco: ASP), 393
Sackett, P. D., Rix, H.-W., Jarvis, B. J., & Freeman, K. C. 1994, ApJ, 436, 629
Sellwood, J. A. 2000, ApJ, 540, L1
Sommer-Larsen, J., & Dolgov, A. 2000, ApJ, submitted (astro-ph/9912166)
Spergel, D. N., & Steinhardt, P. J. 2000, Phys. Rev. Lett., 84, 3760
Springel, V., Yoshida, N., & White, S. D. M. 2000, NewA, submitted (astro-ph/0003162)
Swaters, R. A., Madore, B. F., & Trewhella, M. 2000, ApJ, 531, L107
Tittley, E. R., Couchman, H. M. P., & Pearce, F. R. 1999, MNRAS, submitted (astro-ph/9911017)
Tyson, J. A., Kochanski, G. P., & Dell'antonio, I. P. 1998, ApJ, 498, L107
van den Bosch, F. C., Robertson, B. E., Dalcanton, J. J., & de Blok, W. J. G. 2000, AJ, 119, 1579
van den Bosch, F. C., & Swaters, R. A. 2000, AJ, submitted (astro-ph/0006048)
Weinberg, D. H., Davé, R., Gardner, J. P., Hernquist, L., & Katz, N. 1999, in ASP Conf. Ser. 191, Photometric Redshifts and High-Redshift Galaxies, ed. R. Weymann, L. Storrie-Lombardi, M. Sawicki, & R. Brunner (San Fransisco: ASP), 341
Wyithe, J. S. B., Turner, E. L., & Spergel, D. N. 2000, ApJ, submitted (astro-ph/0007354)
Yoshida, N., Springel, V., White, S. D. M., & Tormen, G. 2000a, ApJ, 535, L103
———. 2000b, ApJ, submitted (astro-ph/0006134)